Ocean Engineering 126 (2016) 299–312

Contents lists available at ScienceDirect

Ocean Engineering

journal homepage: www.elsevier.com/locate/oceaneng

Sea-state based maximum power point tracking damping control of a fully submerged oscillating buoy

Boyin Ding[a,*], Benjamin S. Cazzolato[a], Maziar Arjomandi[a], Peter Hardy[a], Bruce Mills[b]

[a] School of Mechanical Engineering, University of Adelaide, Adelaide, SA 5005, Australia
[b] School of Mathematics and Statistics, University of Western Australia, WA, 6009, Australia

ARTICLE INFO

Keywords:
Maximum power point control
Wave energy convertor
Fully submerged buoy
Tether coupling
Hydraulic PTO
Wave variability

ABSTRACT

Optimal control has been studied for over two decades in the field of ocean wave energy extraction. However, most algorithms require not only extremely detailed models of the plant but also wave prediction, leading to difficulties when implementing these algorithms in reality. This paper investigates the use of maximum power point tracking (MPPT) control – a simple gradient-ascent algorithm well developed for solar and wind energy – on a novel wave energy converter comprising a fully submerged oscillating buoy and a tether coupled hydraulic power-take-off (PTO) unit. A study of the sensitivity of control to irregular wave fluctuations/variability was proposed to systematically determine the step size and update rate of MPPT controller. The world's first commercial scale fully submerged wave energy converter (WEC), Carnegie's CETO system, was used as a test case to assess the proposed methodology under passive damping control. Optimization was done on the CETO system based on typical Australian sea sates in order to benchmark the performance of MPPT control. Simulation results demonstrated that the MPPT damping controlled system is more effective and robust compared to the fixed-damping system with a globally optimized generator damping. The power loss of the MPPT damping controlled system due to tracking and wave/sea state variability is 1.9% of the acausal optimal damping controlled system.

1. Introduction

The ocean presents a promising yet challenging environment for energy extraction. Optimal control for energy extraction is well defined for a wave energy converter (WEC) when using simplified assumptions, such as a monochromatic wave environment, known plant dynamics and linear hydrodynamics (Falnes, 2007). However, a real wave environment, as well as physical WEC constraints such as force, velocity, and position limits, makes a classical optimal approach to WEC control difficult, which may result in suboptimal power extraction or potential damage to the system. Recent work on WEC control, motivated by the difficulty in producing accurate estimation of excitation force, has yielded novel approaches intent on avoiding the prediction problem using non-model based adaptive controllers.

Maximum Power Point Tracking (MPPT) is a non-model based adaptive control algorithm, commonly found in wind and solar energy converters (Koutroulis and Kalaitzakis, 2006; Xiao et al., 2007; van Dam et al., 2012), which uses a gradient-ascent method to optimise power. MPPT control schemes, colloquially referred to as "perturb and observe", work in the WEC power extraction sense by slightly altering an aspect of the power-take-off (PTO) such as the spring stiffness or damping, determining if the perturbation caused the extracted power to increase, and continually perturbing in an attempt to find the point of maximum power. The authors of this paper investigated the performance of MPPT adaptive approach on the latching control of oscillating water column (OWC) (Hardy et al., 2016) under regular/irregular wave conditions. Simulation results demonstrated that system nonlinearities, as well as wave variability, have the potential to result in suboptimal power output for an OWC. Amon et al. (2012) investigated MPPT control for an oscillating body WEC, where the load resistance of a linear generator was tuned by varying the duty cycle of a buck converter. They investigated the effects of varying the update rate and step size of the MPPT algorithm on the average power output of the system for a single sea state. It was concluded that MPPT can successfully find the optimal value of the control parameter and therefore significantly improve average power output of the system in irregular waves. However, there were a number limitations in their study. Firstly, the study only considered a single sea state scenario. Secondly, it was assumed that the instantaneous position of the floating oscillating body is equal to the instantaneous water surface elevation. In other words, the system dynamics are assumed to be that of a "wave follower". The authors stated that this was typical for a device with a

* Corresponding author.
E-mail address: boyin.ding@adelaide.edu.au (B. Ding).

http://dx.doi.org/10.1016/j.oceaneng.2016.09.020
Received 1 September 2015; Received in revised form 8 September 2016; Accepted 12 September 2016

large-diameter float and very high buoyancy (e.g. high hydrostatic stiffness). It is well known that hydrodynamics (e.g. excitation force and radiation force) play a significant role in the absorbed power and therefore the assumption of "wave follower" limited the generality of the study. In addition, the assumption of a linear PTO and heave point absorber further simplified the MPPT control problem because the assumption inherently forced the mapping between the control parameter (e.g. generator duty cycle) and the absorbed power to be convex.

In this paper, a fully submerged oscillating buoy tethered by a hydraulic PTO unit is the system of interest under MPPT control for the following reasons. The oscillating body (buoy) is typically assumed to be partly submerged in literature (Hals et al., 2011; Babarit and Clement, 2006). However, fully submerged WECs are becoming increasingly popular due to their reduced visual impact and increased survivability of storms. The hydrodynamics of fully submerged WECs can differ significantly from partly submerged WECs and must be separately investigated for controller design. In this paper, only the fully submerged case is considered. With regards to the coupling between the oscillating body and the PTO unit, the most common approach in practice is to use a pre-tensioned flexible tether, due to its advantages over a rigid pole connection which is a typical assumption in literature (Vicente et al., 2013; Bachynski et al., 2012). Firstly, the manufacturing/maintenance cost of such a tether is much lower than a rigid pole. Secondly, a tethered coupling makes the underwater installation of the WEC much easier. Finally, a flexible tether coupling allows heave, surge and pitch motions of the oscillating body, resulting in more absorbed power compared to a rigid pole coupling that constrains the absorber to heave motion only (Falnes, 2007). For an axisymmetric body, the use of a tethered coupling leads to a system of three oscillating modes, which in theory requires three tethers to achieve optimal power absorption (Srokosz, 1979; Sergiienko et al., 2016). However, a definitive study on the number of tethers is beyond the scope of this study due to additional control complexity, and therefore, only a single tether scenario is considered. In real-life devices, the most common PTO unit is hydraulic due to their maturity, high power density and robustness. This is an obvious advantage for offshore operations, where maintenance costs can be very high (Henderson, 2006; Cargo et al., 2012; Babarit et al., 2012). However, hydraulic PTO units exhibit nonlinear behaviour. It is likely that the hydraulic nonlinearity would result in non-convex mapping between potential control parameters (e.g. generator resistance) and output power of the generator, consequently degrading the performance of MPPT control. Besides the specific design of the WEC, the variability of real wave conditions is the main factor that can reduce the efficacy of MPPT control. Although this is intuitive, to the best knowledge of the authors, there has been no systematic investigation into this matter so far.

The primary goal of this study is to investigate the capacity of MPPT control on a fully submerged WEC tethered by a generic hydraulic PTO unit under real wave conditions. This will facilitate the applications of MPPT control in common WECs. As part of the work, a high fidelity wave-to-wire model was developed for the simulation study based on the well-known Cummins model with additional non-linear damping (Morison's formula). The nonlinear behaviour of the hydraulic system was considered in modelling. A sea-state based MPPT damping control strategy was formulated for a generic hydraulic PTO system. The proposed control strategy is fully passive, and therefore can be easily applied to a generic hydraulic PTO unit that can only operate in power generator mode (Hals). The world's first commercial-scale fully submerged WEC, Carnegie's CETO, was used as an example to present the simulation results.

2. Wave-to-wire model

A simplified WEC model consisting of a fully submerged cylindrical buoy and a hydraulic PTO unit is shown in Fig. 1. A pre-tensioned tether (2) connects the buoy to a single-acting hydraulic pump (3) that is part of the hydraulic PTO unit. Universal joints are placed at the mooring point of the hydraulic pump (C) and at the attachment point on the buoy (A), allowing the buoy (1) to move freely in the plane of the incoming wave. The motion of the buoy drives the hydraulic pump. The resulting motion of the pump piston relative to the pump cylinder drives fluid through a set of two check valves (4) to rectify the flow so that fluid always passes through the hydraulic motor in the same direction (independent of the direction of the buoy motion). A high pressure accumulator (5) is placed on the inlet to the hydraulic motor and a low pressure one (6) on the outlet of the hydraulic motor. The pressure difference between the two accumulators drives the hydraulic motor (7), which is connected to an electrical generator. The accumulators are included in the hydraulic PTO unit to keep an approximately constant pressure differential across the motor so it rotates at an approximately constant speed, and therefore, energy is transmitted at approximately a constant rate.

2.1. Dynamics model of the WEC

Assuming an incompressible fluid with zero viscous losses, linear wave theory can be used to solve the governing hydrodynamic equations. It is well known that linear wave theory is not capable of modelling the higher order dynamics of buoy-fluid interaction and may result in overestimation of the power absorption capacity of the WEC, particularly at high sea states (Falnes, 2007). Nevertheless, it is an effective computational tool for the study of control methods applied to WECs and is sufficient to analyse control systems. The dynamic equation for the buoy motion is (Falnes, 2007)

$$\mathbf{M}\ddot{\boldsymbol{x}} + \boldsymbol{F}_{\mathrm{r}} + \boldsymbol{F}_{\mathrm{hs}} = \boldsymbol{F}_{\mathrm{e}} + \boldsymbol{F}_{\mathrm{drag}} + \boldsymbol{F}_{\mathrm{m}}, \tag{1}$$

where $\boldsymbol{x}$ is a displacement vector that represents the surge x, heave z, and pitch θ motions of the buoy at the centre of gravity (COG),

$$\boldsymbol{x} = [x \quad z \quad \theta]^{\mathrm{T}}; \tag{2}$$

$\mathbf{M}$ represents the buoy mass matrix with the buoy mass m, and moment inertia I, at its diagonal axis

$$\mathbf{M} = \begin{bmatrix} m & 0 & 0 \\ 0 & m & 0 \\ 0 & 0 & I \end{bmatrix}; \tag{3}$$

$\boldsymbol{F}_{\mathrm{e}}$, the excitation force, is the force produced by the incident waves on an otherwise fixed body; The radiation force, $\boldsymbol{F}_{\mathrm{r}}$, is the force produced by an oscillating body creating waves on an otherwise calm sea; $\boldsymbol{F}_{\mathrm{hs}}$ is the hydrostatic fore; $\boldsymbol{F}_{\mathrm{drag}}$ is the form drag force; $\boldsymbol{F}_{\mathrm{m}}$ represents the PTO force acting at the buoy COG. Based on the schematics shown in Fig. 1, $\boldsymbol{F}_{\mathrm{m}}$ can be written as

$$\boldsymbol{F}_{\mathrm{m}} = \mathbf{T}\boldsymbol{F}_{\mathrm{PTO}}, \tag{4}$$

where $\boldsymbol{F}_{\mathrm{PTO}}$ is a vector denoting the PTO force along the tether and $\mathbf{T}$ represents the matrix which transports the PTO force applied at the attachment point to the buoy COG

$$\mathbf{T} = \begin{bmatrix} 1 & 0 & 0 \\ 0 & 1 & 0 \\ -d\cos(\theta) & d\sin(\theta) & 1 \end{bmatrix}, \tag{5}$$

where, d is the distance between the attachment point (A) and the buoy COG (G). It is worth noting that $\boldsymbol{F}_{\mathrm{m}}$ is a nonlinear function due to both tether attachment and hydraulic PTO behaviour (e.g. valve switching, pressure losses). Therefore, analysis of the system must be conducted in the time domain. Cummins (Cummins, 1962) developed a time-domain approach for investigating ship response to sea waves, which has been widely applied and accepted when investigating WECs. With this approach, the equation of motion takes the following form (Cummins, 1962)

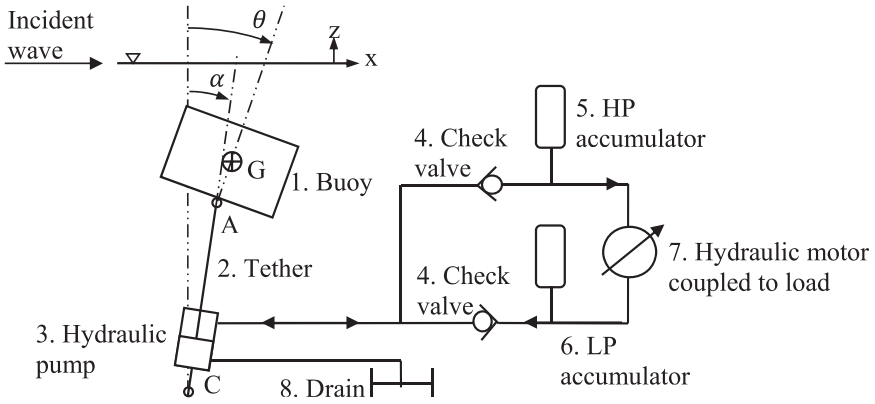

Fig. 1. A generic WEC model consisting of a submerged cylindrical buoy, hydraulic PTO unit and tether coupling.

$$(\mathbf{M}+\mathbf{A}_\infty)\ddot{\boldsymbol{x}}(t)+\int_0^t \mathbf{B}(t-\tau)\dot{\boldsymbol{x}}(t)d\tau+\boldsymbol{F}_{\rm hs}=\boldsymbol{F}_{\rm e}+\mathbf{T}\boldsymbol{F}_{\rm PTO}+\boldsymbol{F}_{\rm drag}, \tag{6}$$

where $\mathbf{A}_\infty$ is the infinite added mass matrix whose diagonal elements represent the limiting value of the added mass term of the radiation force (e.g. $\mathbf{A}_\omega$ for $\omega=\infty$). The convolution product $\int_0^t \mathbf{B}(t-\tau)\dot{\boldsymbol{x}}(t)d\tau$ represents the memory effect of the radiation force, which is dependent on the history of the buoy motion. Each diagonal element of $\mathbf{B}(t)$ is an impulse response function that depends essentially on the shape of the buoy and can be computed directly in the time domain by using dedicated seakeeping BEM code like ACHIL3D (Babarit and Clement, 2006). However, solving the convolution product can be a tedious process. One way to overcome this is to approximate the convolution term by a linear time-invariant model (Hals). In (Perez and Fossen, 2009), a Matlab toolbox was developed to identify the fluid-memory model of the radiation force as a transfer function given the frequency-dependent hydrodynamic coefficients (e.g. added mass $\mathbf{A}(\omega)$ and radiation resistance $\mathbf{B}(\omega)$). The identified transfer function can then be converted to a state-space model for use in time-domain by using standard Matlab command 'tf2ss'. The excitation force $\boldsymbol{F}_{\rm e}$ is expressed as the product of wave elevation η at the centre axis of the buoy and excitation force coefficients $\boldsymbol{H}_{\rm ex}$ in frequency domain as

$$\boldsymbol{F}_{\rm e}(\omega)=\boldsymbol{H}_{\rm ex}(\omega)\eta(\omega). \tag{7}$$

Alternatively the excitation force can be expressed as a convolution product of the two in time domain simulations,

$$\boldsymbol{F}_{\rm e}(t)=\int_0^t \boldsymbol{H}_{\rm ex}(t-\tau)\eta(t)d\tau(t). \tag{8}$$

The excitation force coefficient depends on the buoy geometry and is in general non-causal (Falnes, 2007). Thus, it is difficult to compute the excitation force time series using a state-space approximation of the excitation-term convolution in the same manner as for the radiation-term convolution (Hals). Prediction or measurement of the wave elevation must be provided some time into the future. Instead of using the wave elevation as input, one can in time-domain simulations use the excitation force directly, which can then be pre-calculated based on the frequency dependent excitation force coefficients $\boldsymbol{H}_{\rm ex}(\omega)$ (Vicente et al., 2013). Frequency-dependent hydrodynamic coefficients $\mathbf{A}(\omega)$, $\mathbf{B}(\omega)$ and $\boldsymbol{H}_{\rm ex}(\omega)$ can be computed directly by using dedicated computer code like WAMIT (Babarit and Clement, 2006). For regular shape buoys (e.g. sphere or cylinder), frequency-dependent hydrodynamic coefficients can be computed by using semi-analytical methods described in (Srokosz, 1979; Jiang et al., 2014). WAMIT was used in this study. In the case of a monochromatic incoming wave, the time series of the excitation force can be written as

$$\boldsymbol{F}_{\rm e}(t)=\boldsymbol{H}_{\rm ex}(\omega)\bullet A\bullet\sin(\omega t), \tag{9}$$

where A is the amplitude of the wave elevation and ω is the frequency of the incoming wave. Thus the excitation force time series is a sinusoidal waveform that has the same frequency of the incoming wave but different amplitude and phase. In the case of irregular incoming waves, if the spectrum for the incoming wave $S_\eta(\omega)$ is known, a good approximation to the excitation force can be constructed by summing components made from the discretised wave spectrum (Hals). For frequency component k corresponding to angular frequency $\omega_k=k\Delta\omega$, the complex wave elevation amplitude of the evenly spaced wave elevation spectrum $S_{\eta,k}=S_\eta(k\Delta\omega)$ can be found by (Hals)

$$\eta_k=\sqrt{2S_{\eta,k}\Delta\omega}\,e^{j\varphi_{\eta,k}}, \tag{10}$$

where the phase information of the wave elevation $\varphi_{\eta,k}$ is either known from measurements or has been synthesised with random phase components. The complex amplitude of the excitation force can be computed by the use of the excitation force coefficients $\boldsymbol{H}_{\rm ex}(k\Delta\omega)$

$$\boldsymbol{F}_{{\rm e},k}=\boldsymbol{H}_{\rm ex}(k\Delta\omega)\eta_k. \tag{11}$$

With N frequency components, the excitation force time series is now calculated as

$$\boldsymbol{F}_{\rm e}(t)=\sum_{k=1}^{N}\Re\{\boldsymbol{F}_{{\rm e},k}e^{jk\Delta\omega t}\}. \tag{12}$$

Various mathematical models have been proposed and used for analytical representation of real-sea spectra $S_\eta(\omega)$, of which the most commonly used are the JONSWAP, Bretschneider and Pierson-Moskowitz spectra (Ringwood et al., 2014). The hydrostatic force $\boldsymbol{F}_{\rm hs}$ in Eq. (6) represents the net restoring force due to buoyancy and gravitational forces and takes the form

$$\boldsymbol{F}_{\rm hs}=(\rho V_{\rm b}-m)\boldsymbol{g}, \tag{13}$$

where ρ is the density of the sea water, $V_{\rm b}$ is the total volume of the buoy, $\boldsymbol{g}$ is the gravitational vector. The hydrostatic force is a positive constant that maintains a tension force on the tether. $\boldsymbol{F}_{\rm PTO}$ in Eq. (6) is the PTO force vector along the tether, which can be written as

$$\boldsymbol{F}_{\rm PTO}=f_{\rm hd}\begin{bmatrix}\sin(\alpha)\\ \cos(\alpha)\\ 0\end{bmatrix}, \tag{14}$$

where $f_{\rm hd}$ is the force arising from the impedance of the hydraulic PTO unit, and is controllable via tuning some aspects of the hydraulic system. Hydraulic PTO modelling and tuning is discussed in Section 2.2. The variable α is the angle of the tether with respect to the vertical z direction as seen in Fig. 1. The angle α can be calculated from the buoy displacement

$$x_{\rm a}(t)=x(t)-d\sin(\theta) \tag{15}$$

$$z_{\rm a}(t)=z(t)-d\cos(\theta) \tag{16}$$

$$\alpha=\arctan\left(\frac{x_{\rm a}(t)}{z_{\rm a}(t)}\right), \tag{17}$$

where $x_a(t)$ and $z_a(t)$ are respectively the horizontal and vertical displacement of the attachment point on the buoy (A). The elongation velocity of the tether and consequently the velocity of the hydraulic pump piston can be obtained by differentiating the elongation displacement of the tether

$$\dot{l}=\frac{d\left(\sqrt{(z_a(t)-z_c)^2+(x_a(t)-x_c)^2}\right)}{dt}, \tag{18}$$

where x_c and z_c are respectively the position of the mooring point (C) of the hydraulic pump in the horizontal direction and in the vertical direction. The rate $\dot{l}$ is used to compute hydraulic PTO force f_{hd}. The computation of the form drag force $\boldsymbol{F}_{drag}$ in Eq. (6) is given by (Rafiee and Fievez):

$$\boldsymbol{F}_{drag}=\begin{pmatrix} -\frac{1}{2}\rho C_{Dx}A_x|\dot{x}|\dot{x} \\ -\frac{1}{2}\rho C_{Dz}A_z|\dot{z}|\dot{z} \\ -\frac{1}{2}\rho C_{D0}D^5|\dot{\theta}|\dot{\theta} \end{pmatrix} \tag{19}$$

where C_{Dx}, C_{Dz}, and C_{D0} are the drag coefficients of the buoy along surge, heave and pitch axes, respectively; A_x and A_z are the cross-section areas of the buoy along surge and heave axes, respectively; and D is the diameter of the buoy. The drag coefficients are normally obtained from numerical wave tank testing for the shape of the buoy of interest (Rafiee and Fievez). In Eq. (19), the effects of surrounding water particle velocities on the drag force are ignored given their negligible influence on the system.

2.2. Hydraulic PTO model

A simplified analytical model of the hydraulic PTO unit shown in Fig. 1 is described in (Cargo et al., 2012; Babarit et al., 2009; Falcao and de, 2007). The corresponding equations are excluded from this document to avoid repetition. This study used the Simscape SimHydraulic toolbox in Mathworks Simulink to model the hydraulic PTO system. A snapshot of the model is shown in Fig. 2. The blocks for the hydraulic pump, the tuning accumulator, and the pipelines are highlighted in the red box. The hydraulic pump piston velocity $\dot{l}$ is the input of the model that drives the hydraulic flow in the pipeline. The tuning accumulator near the hydraulic pump is used to balance the net buoyancy force of the buoy at the start of the simulation. The whole hydraulic PTO unit is assumed to be located into the inner space of the oscillating buoy, and consequently hydraulic fluid inertia is negligible. The "hydraulic pipeline" block allows the definition of the dimensions of the hydraulic pipeline delivering power to the hydraulic motor, thus capturing fluid compressibility in the pipeline. The blocks for the accumulators on the high and low pressure lines as well as the check valves are highlighted in the yellow box. The thermodynamic transformations in the accumulators are assumed to be isentropic, which is reasonable considering the cycle time in the device. The blocks for the hydraulic motor and the power generator are highlighted in the blue box. The electrical generator coupled to the hydraulic motor delivers power ashore via electrical cable. The generator is modelled as a simple rotational damper with varying damping coefficient. This means that the resistive torque imposed by the generator can be altered by varying this damping coefficient. Consequently, the differential pressure through the hydraulic motor can be controlled. Modelling the generator as a pure damper is for the ease of control. Nonlinear behaviour of the electrical generator may cause local maxima in maximum power tracking. Therefore, in practice, rather than maximizing the electrical power, maximizing the mechanical power is preferred from the control point of view. A bi-directional pump, highlighted in the cyan box, is included to enable control of the total fluid volume in the system. Changing the total volume of fluid changes the fluid level inside the accumulators and therefore changes the mean pressure in the system. An "ideal force sensor" block in the red box computes the hydraulic PTO force f_{hd} and feeds it back to Eq. (14) to compute the PTO force vector. The instantaneous electrical power produced by the PTO is

$$P_{inst}=T_g\omega_g, \tag{20}$$

where T_g is the generator torque and ω_g is the generator speed. The mean power output of the PTO unit is

$$P_m=\frac{1}{N_p}\sum_{i=1}^{N_p}P_{inst,i}, \tag{21}$$

where $P_{inst,i}$ is the discrete instantaneous PTO power sampled at a fixed sample rate f_s, and N_p is the number of stored instantaneous PTO power samples. The generator damping coefficient d_m and fluid volume V_f are used as the control parameters to optimise the mean power output of the unit. The power map against the change of these two control parameters, e.g. $P_m=f(d_m, V_f)$, will be investigated in the following sections under various irregular wave conditions. The hydraulic PTO model was validated against a simplified PTO model provided by Carnegie Wave Energy Limited, where a constant pressure difference is assumed between the high pressure line and low pressure line of the hydraulic circuit.

3. Sea-state based MPPT control

Maximum Power Point Tracking (MPPT) is a gradient ascent type algorithm which maximises mean power with respect to a chosen variable. The MPPT algorithm concept is based on continually perturbing one or more system variables and observing the associated changes in power. The objective is to find the values of the variables that result in maximum power. For MPPT to be effective, the power vs. perturbed variable map, $P=f(\gamma)$, should be convex with a well-defined global maxima occurring at γ_{opt}, as then MPPT will continually perturb γ such that $\gamma\rightarrow\gamma_{opt}$, increasing and ideally maximizing mean power. The gradient ascent MPPT control algorithm takes the form (Xiao et al., 2007)

$$\gamma_i(k+1)=\gamma_i(k)+K\left(\frac{\partial P}{\partial\gamma_i}\right)_{\gamma_i=\gamma_i(k)} \tag{22}$$

for $i=$ 1: number of elements in γ, with index k denoting the iterations, and a scalar parameter $K>0$ being a scaling factor. The gradients can be approximated through first-order backward differencing

$$\left(\frac{\partial P}{\partial\gamma_i}\right)_{\gamma_i=\gamma_i(k)}\approx\frac{P(k)-P(k-1)}{\gamma_i(k)-\gamma_i(k-1)}. \tag{23}$$

Another common MPPT approach is to use fixed-step optimization to update the control variables, also known as hill-climbing optimization (Xiao et al., 2007)

$$\gamma_i(k+1)=\gamma_i(k)+\mu\bullet\mathrm{sign}\left(\left(\frac{\partial P}{\partial\gamma_i}\right)_{\gamma_i=\gamma_i(k)}\right) \tag{24}$$

with a small scalar $\mu>0$ defining the fixed size of the increment steps on γ_i at each iteration. Compared to the gradient-ascent MPPT method, the fixed-step MPPT method has a slower dynamic response and a more oscillatory behaviour at steady-state but is less sensitive to fluctuations and noise in the power production (Xiao et al., 2007; van Dam et al., 2012). Both MPPT control algorithms can be tuned in two aspects: the update rate of the iteration f_{update} and the scaling factor K or the step size μ. The update rate controls the rate at which the controller responds to changes in the mean power output. It also determines the number of samples, N_p, used in calculating the average of the power output given by

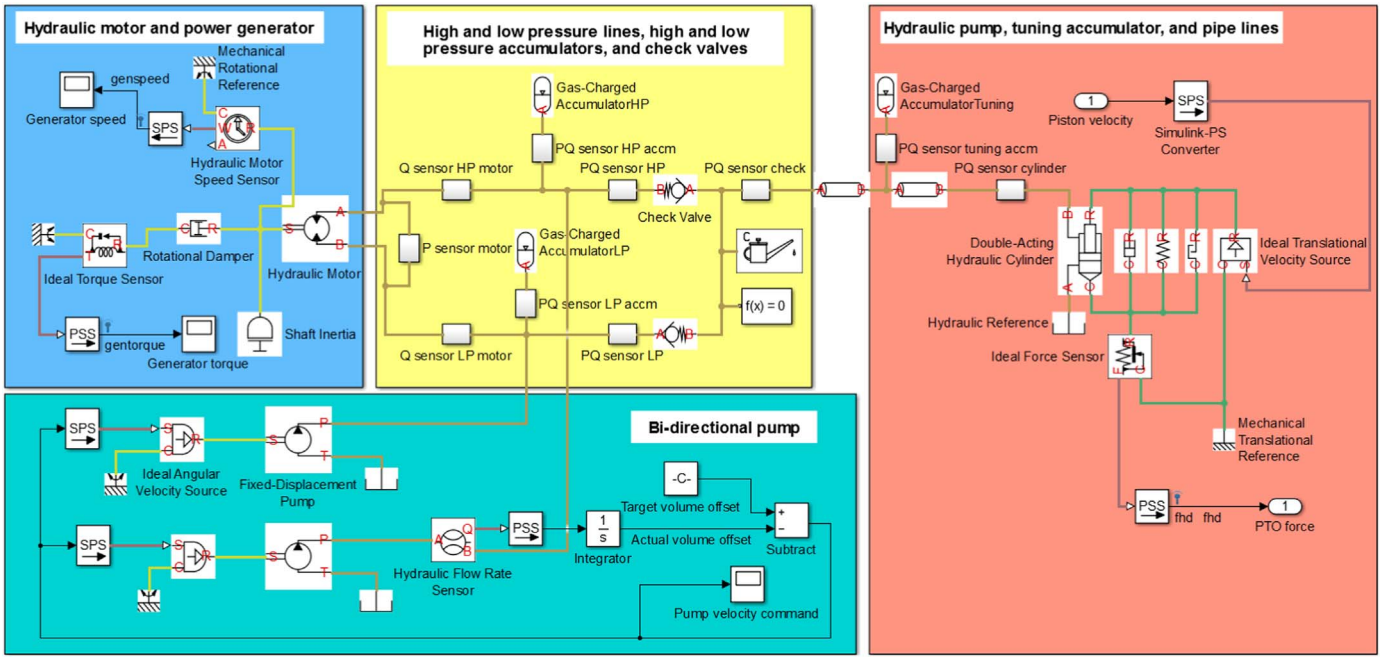

Fig. 2. Hydraulic PTO Simscape model.

$$N_p=\frac{f_s}{f_{\text{update}}}. \tag{25}$$

A fast update rate is desirable for the controller to respond quickly to changes in environment (e.g. changes in incoming wave conditions or sea states). However, the update rate is also inversely proportional to the amount of new information used to influence the next controller action. If the update rate is too fast there may be insufficient new information to optimise power extraction. The scaling factor or the step size controls the resolution of the MPPT algorithm and determines how aggressively the controller responds to changes in the mean power output. The tuning of this parameter should compromise the trade-off between power oscillation and slow power convergence, both of which can degrade the mean power output. Typically, selection of the update rate and the scaling factor or the step size is a trial-and-error exercise (Xiao et al., 2007).

In general, the mean power output of the system, P_m, is a function of the uncontrollable and controllable variables

$$P_m=f(\boldsymbol{\beta}, \boldsymbol{\gamma}), \tag{26}$$

where the controllable variables γ are the variables (e.g. the generator damping coefficient or the fluid volume in the hydraulic PTO) that can be actively controlled using MPPT. The uncontrollable variables β are the variables (e.g. the amplitude and frequency of the incident wave elevation) that change with environment changes. For the MPPT method to be effective, the change in the mean power output due to uncontrollable variable change needs to be smaller than the change in the mean power output due to controllable variable change, e.g.,

$$\sum_{j=1}^{M_\beta}\frac{\partial P_m}{\partial \beta_j}<\frac{\partial P_m}{\partial \gamma_i}, \tag{27}$$

where M_β denote the number of elements in β. In the applications of solar and wind energy conversion, the aforementioned relationship is satisfied most of time due to the slow varying nature of solar and wind. However, it is not the case in the applications of wave energy conversion given the fast fluctuating/varying nature of ocean waves, even under a single sea state. Therefore, a sensitivity study needs to be undertaken for irregular wave conditions, to determine the suitable update rate and step size based on Eq. (27). The sensitivity study is discussed in Section 6. In addition, sea state variability can further degrade the performance of MPPT control as it is well known that MPPT controllers can become confused in changing environment conditions (Hardy et al., 2016). Therefore, the authors proposed to replace the mean power output with mean capture width, which inherently contains information regarding the changing environment, and use the mean capture width as the optimization target in the MPPT algorithm for wave energy conversion applications. Consequently, Eqs. (22) and (24) can be re-written as

$$\gamma_i(k+1)=\gamma_i(k)+K\left(\frac{\partial W_m}{\partial \gamma_i}\right)_{\gamma_i=\gamma_i(k)} \tag{28}$$

$$\gamma_i(k+1)=\gamma_i(k)+\mu\bullet\text{sign}\left(\left(\frac{\partial W_m}{\partial \gamma_i}\right)_{\gamma_i=\gamma_i(k)}\right), \tag{29}$$

where the mean capture width W_m represents the ratio of the mean power output P_m to the energy transport of the incident wave per unit width of wave frontage J_r (Falnes, 2007). For irregular incident waves, the mean capture width is

$$W_m=\frac{P_m}{J_r}=\sum_{i=1}^{N_p}\left(\frac{4\omega_i}{\rho g^2 D(k_i h)A_i^2}\right)P_m, \tag{30}$$

where A_i is the amplitude of the wave elevation spectrum obtained from Fast Fourier Transform, ω_i is the frequency component of the incoming wave, ρ is the density of sea water, g is the gravitational acceleration, k_i is the wavenumber, h is the depth of water, and $D(kh)=\tanh(kh)+kh-(kh)\tanh^2(kh)$ is the depth function (Falnes, 2007). It can be seen that the mean capture width normalises the mean WEC power output with the energy transport of the incident wave, consequently providing the controller with the knowledge regarding environmental disturbances (e.g. sea state change). In real-time control, the computation of the wave elevation spectrum requires the measurement of the instantaneous wave elevation using wave probes.

Based on the sensitivity study for irregular waves and the concept of using capture width for optimization, this study developed a sea-state based MPPT control method for use in a generic non-reactive hydraulic PTO unit, where the time constants for varying accumulator pressures are slow. The fixed-step MPPT algorithm forms the fundamental basis

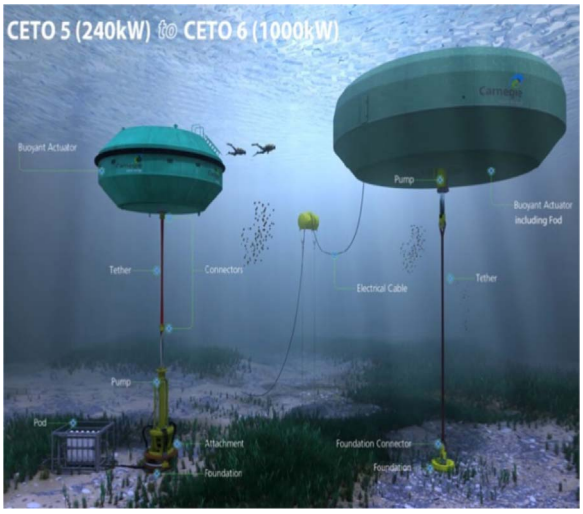

Fig. 3. CETO 5 (left) and CETO 6 3D model (Carnegie Wave Energy, 2014).

given its inherent robustness to wave fluctuations. Using the generator damping coefficient d_m as the control parameter, the fixed-step MPPT algorithm takes the form

$$d_m(k+1)=d_m(k)+\mu_d \cdot \text{sign}\left(\frac{W_m(k)-W_m(k-1)}{d_m(k)-d_m(k-1)}\right), \quad (31)$$

where μ_d represents the step size of the generator damping coefficient. The update rate is denoted as f_d. Typically, the inverse of the update rate must be set to a constant greater than that of the time constant of the system, so as to prevent instability (Snyder, 2000; Elmes, 2007). The actuation latency in varying the control parameter (e.g. pumping fluid into the hydraulic PTO unit) needs to be considered in the computation of the system time constant.

4. Carnegie CETO system

Carnegie's CETO WEC is the first fully-submerged commercial unit to produce high pressure water from the power of waves. The fully-submerged nature of the system leads to zero visual impact as well as strong survivability during storms. Three CETO 5 units (pictured on left hand side of Fig. 3), each generating a rated capacity of approximately 240 kW, were successfully installed at Perth Wave Energy Project Site off Garden Island, Western Australia, and have been operated for over 12 months, delivering significant amounts of real-time data, which is critical to validate Carnegie's proprietary computational models (Rafiee and Fievez). These models can then be used with confidence in finalising the design of Carnegie's 1 MW CETO 6 system (pictured on right hand side of Fig. 3) by the end of 2016.

5. Optimization of CETO control parameters

This work will consider MPPT control of a 1 MW submerged WEC, similar to the configuration of Carnegie's CETO 6 design, with model parameter settings listed in Table 1. It is worth noting that these parameters do not represent the ones which will be used in the final CETO 6 design, however, they are indicative. As shown in Fig. 3, the geometry of the CETO buoy is similar to a circular cylinder with chamfered edges to reduce drag forces as well as vortex shedding. The hydrodynamic coefficients of the CETO buoy computed from WAMIT under linear wave theory (to be used for simulation in this paper) are almost identical to that of a circular cylinder buoy with the same dimensions. Therefore, it is expected that a simplified cylindrical buoy can produce similar results, at least under the assumption of linear wave theory. The submergence depth refers to the distance between the water surface and the buoy top surface when the buoy reaches its highest possible position (governed by the PTO stroke limit). When the buoy is at its nominal position, the top surface of the buoy is 3.5 m below the water surface. In WAMIT, convergence tests were conducted to minimize mesh discretization errors and consequently assure the accuracy of the hydrodynamic coefficients output. The mesh was refined at the sharp edges, leading to a total 5792 panels on the surface of the CETO buoy. Since the exact shape of CETO buoy is confidential, the authors are unable to disclose mesh discretization. The drag coefficients of the CETO buoy were determined from numerical wave tank testing using computational fluid dynamics (CFD) simulation as described in Rafiee and Fievez. The developed wave-to-wire model has been benchmarked to a simplified model, where a cylindrical buoy is connected to a simplified analytical hydraulic PTO, and was found to be valid for the following optimization and control studies, at least under the assumption of linear wave theory.

Table 1
Model parameters.

Buoy property	Value	PTO property	Value
Height	6 m	Tether length	13.5 m
Diameter	20 m	Pump stroke	6 m
Volume	1760 m^3	Pump piston area	0.4 m^2
Mass	1.25 kt	Accumulator volume	5 m^3
Submergence depth	0.5 m	Motor displacement	0.00014 m^3/rad
Water depth	30 m	Motor efficiency	0.8

5.1. Optimization based on individual sea state

Optimization of the generator damping coefficient and fluid volume was conducted under irregular incident waves with significant wave height from 1 m to 6 m in 1 m increments and with peak wave period from 6 s to 17 s in 1 s increments. Wave heights and periods were selected based on standard Australian sea states (Hemer and Griffin, 2010). Pierson-Moskowitz spectra were used to describe each of the sea states. During optimization, the generator damping coefficients were varied from 0.25 to 7.5 Nm/(rad/s) with increments of 0.25 Nm/(rad/s). The fluid volume in the hydraulic system was normalized to an offset with respect to the nominal fluid volume. At nominal conditions, the initial volume of the accumulators are set to counteract the static buoyancy force of the buoy. The fluid volume offset was varied between −1.4 and 4.4 m^3 with increments of 0.2 m^3. Each individual case was run for 320 cycles of the peak wave period. Such run durations were chosen based on the sensitivity study covered in Section 6. Instantaneous electrical power was averaged based on the data collected between the 20th and 320th cycles of the peak wave period to exclude transient behaviour at the beginning of the simulation. The fluid volume of the system was set to nominal (with zero offset) when the effects of varying the generator damping coefficient are investigated. The averaged generated power against generator damping coefficients for irregular waves of 2 m significant wave height and various peak wave periods is shown in Fig. 4. The optimal generator damping coefficients that achieve the maximum averaged power are sensitive to the changes in peak wave periods. This means that the generator damping coefficient needs to be varied/controlled to maximize power absorption from ocean. The use of a fixed generator damping coefficient is optimal for some peak wave period, but can result in up to 30% power loss for some peak wave periods investigated as evident in Fig. 4. The averaged generated power against generator damping coefficients subjected to irregular waves of 12 s peak wave period and various significant wave heights is shown in Fig. 5. The optimal damping coefficient is relatively insensitive to the changes in significant wave heights. The function of averaged generated power against generator damping coefficient is convex as shown in Figs. 4 and 5, which is ideal from the control point of view. The relative capture width of the device at optimal generator

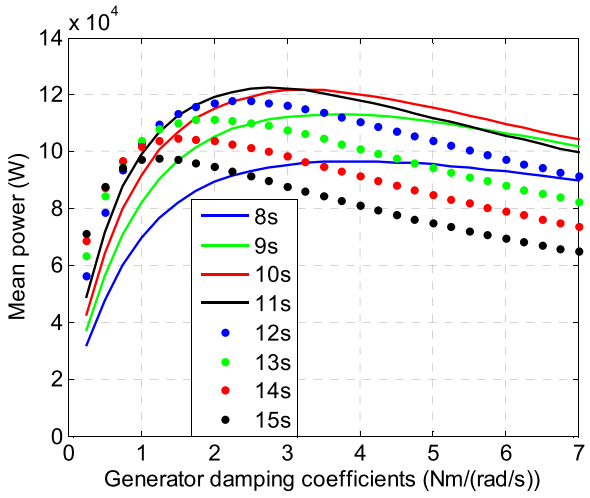

Fig. 4. Averaged generated electrical power versus generator damping coefficients subjected to irregular waves of 2 m significant wave height and various peak wave periods: 8 s, 9 s, 10 s, 11 s, 12 s, 13 s, 14 s and 15 s.

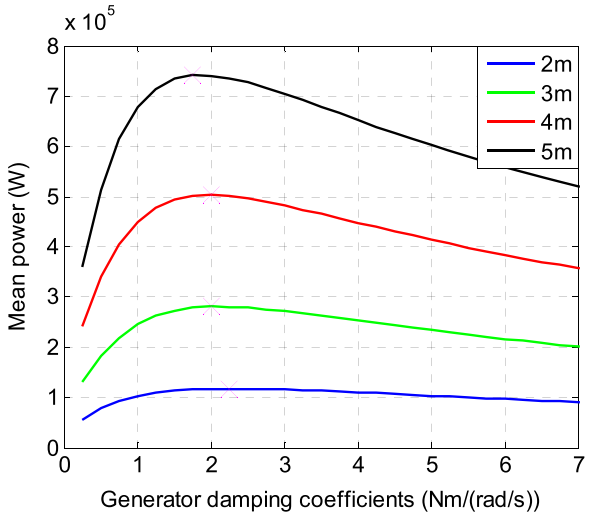

Fig. 5. Averaged generated electrical power versus generator damping coefficients subjected to irregular waves of 12 s peak wave period with various significant wave heights: 2 m, 3 m, 4 m, 5 m. The pink x-marks represent the optimal points.

damping coefficients at various significant wave heights and peak wave periods is shown in Fig. 6. The relative capture width reaches a maximum (0.34) for short wave periods of 9 s and a minimum (0.18) for long wave periods of 15 s. The relative capture width of the device considered is similar in magnitude to that of a standard heaving buoy, as most of the energy captured by the device is due to the heaving motion (Ding. et al.). The relative capture width decreases with an increase in the peak wave period since power of incident wave increases with an increase in the peak wave period, and consequently the peak wave period at which the relative capture width reaches maximum does not represent the resonance period of the wave energy converter (at approximately 10–11 s as evident in Fig. 4). The optimal damping coefficients at various significant wave heights and peak wave periods are shown in Fig. 7, where it is evident that the optimal damping coefficient decreases with increasing peak wave period.

The generator damping coefficient was fixed at its optimal value for each sea state when the effects of varying the fluid volume in the hydraulic system are investigated. The dependence of averaged generated power on fluid volume offset is shown in Fig. 8 for irregular waves of 2 m significant wave height and various peak wave periods. From Fig. 8, it is evident that the optimal fluid volume offset that results in the maximum average power is not particularly sensitive to the change

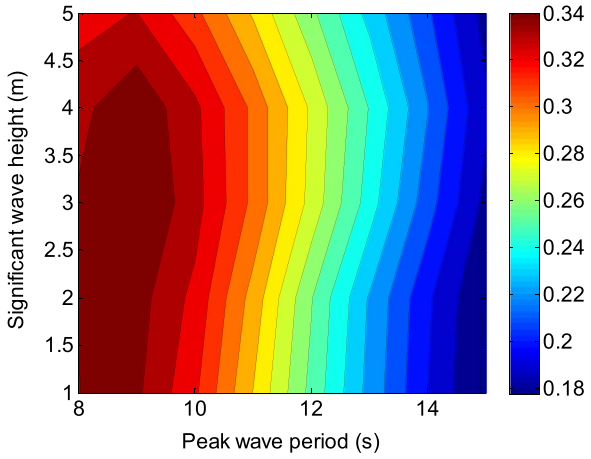

Fig. 6. Maximum relative capture width (at optimal damping for each sea state) of the device versus significant wave heights and peak wave periods.

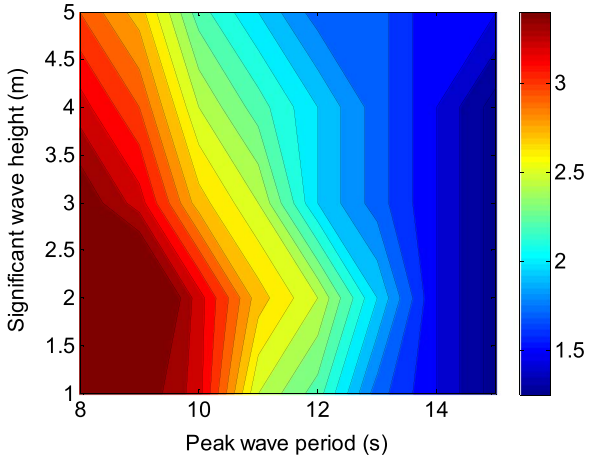

Fig. 7. Optimal generator damping (Nm/(rad/s)) for each sea state versus significant wave heights and peak wave periods.

of peak wave period. The averaged generated power against fluid volume offset for irregular waves of 12 s peak wave period and various significant wave heights is shown in Fig. 9. From Fig. 9, it is evident that the optimal fluid volume offset slightly decreases with an increase in the significant wave height for significant wave heights exceeding 4 m. In continental Australia, significant wave height higher than 4 m rarely occur. Thus, it is not necessary to dynamically control the fluid volume within the hydraulic PTO system.

5.2. Optimization based on single site

The probability of occurrence of sea states varies with site in which the WECs operate. Two sites along the coast of Australia were selected to assess the efficiency of the CETO device. One site is located at Cape Naturaliste (CN), Western Australia (114.80E, 33.50S) and the other site is located near Sydney, New South Wales (152.50E, 34.00S). The sea state data between 1979 and 2010 associated with these two sites were provided by the Commonwealth Scientific and Industrial Research Organisation (CSIRO). The sea state occurrence probability diagram at the above two mentioned sites is shown in Figs. 10 and 11, with the peak wave periods and significant wave heights quantized to integers.

The global optimal generator damping, assuming no control and constant damping applied across all sea states, can be determined considering the probability of sea state occurrence by finding the fixed damping that yields maximum average power across all sea states for the site of interest. This power level, $\bar{P}_{fd}$, represents the maximum

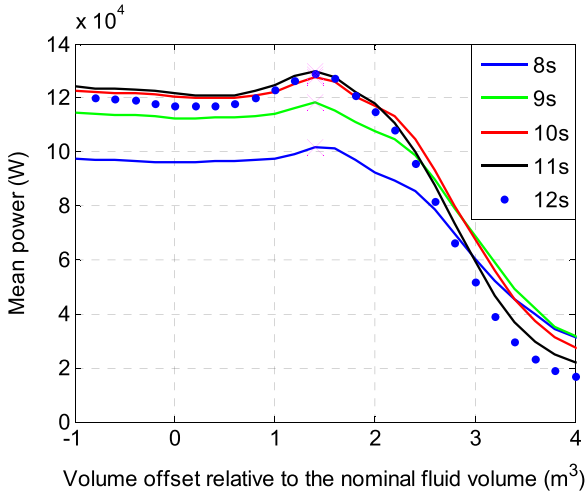

Fig. 8. Averaged generated electrical power versus fluid volume offset subjected to irregular wave of 2 m significant wave height and various peak wave periods: 8 s, 9 s, 10 s, 11 s and 12 s. The pink x-marks represent the optimal points.

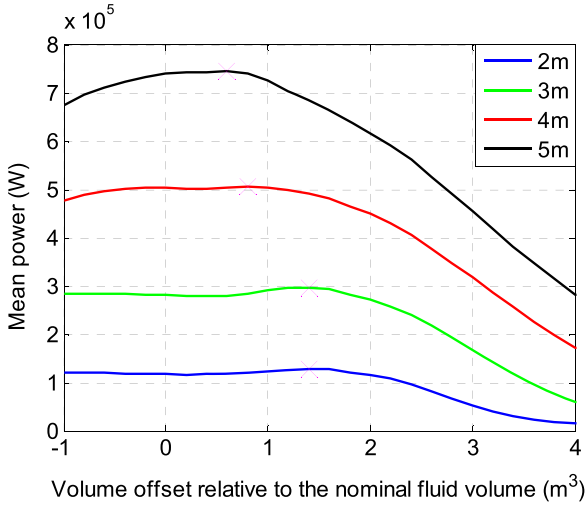

Fig. 9. Averaged generated electrical power versus fluid volume offset subjected to irregular waves of 12 s peak wave period with various significant wave heights: 2 m, 3 m, 4 m, 5 m. The pink x-marks represent the optimal points.

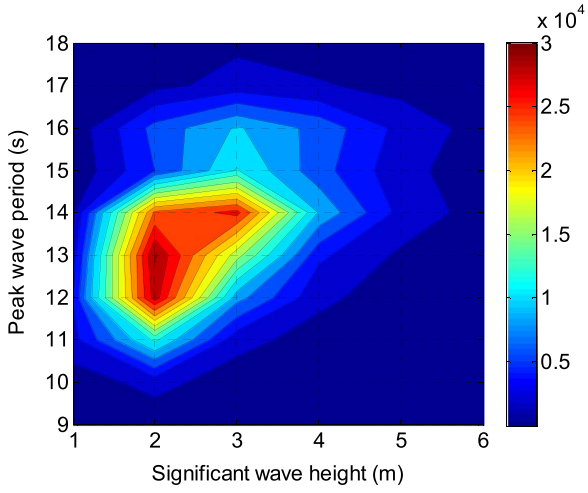

Fig. 10. Scattering diagram shows the occurrence probability of sea states between 1979 and 2010 at Cape Naturaliste, Western Australia. The color bar represents the number of hours of occurrence over the entire period.

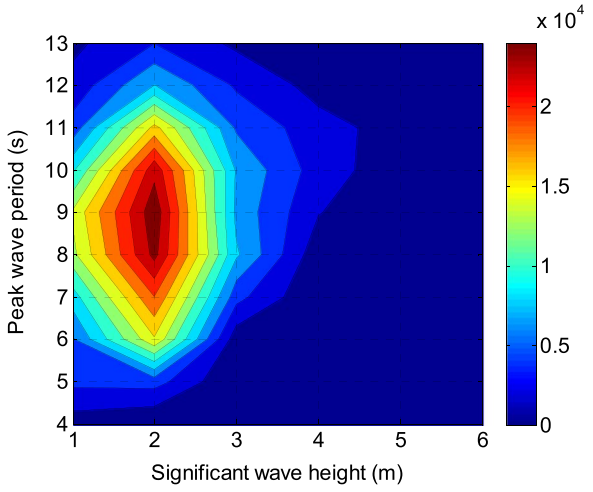

Fig. 11. Scattering diagram shows the occurrence probability of sea states between 1979 and 2010 near Sydney, New South Wales.

Table 2
Maximum efficiency of the device at the two selected sites.

Site	Fixed-damping system		Optimal damping controlled system
	Maximum averaged power, $\bar{P}_{fd}$ (kW)	Global-optimal damping (Nm/(rad/s))	Averaged power, $\bar{P}_{odc}$ (kW)
CN (114.80E, 33.50S)	220	1.75	224
Sydney (152.50E, 34.00S)	122	2.75	124

amount of power that can be theoretically extracted from a fixed-damping system. Additionally, the optimal damping for each sea state can be determined, and consequently considering the probability of sea state occurrence the averaged power arising from optimal damping control can be determined. This power level, $\bar{P}_{odc}$, represents the amount of power that can be extracted from a perfect/optimal sea-state based passive damping controlled system, and thus exceeds $\bar{P}_{fd}$. The power efficiency of the CETO device at the CN site and Sydney site is shown in Table 2, with fixed generator damping and optimal damping control respectively. At the CN site, the averaged power extracted from a globally optimized fixed-damping system and from an optimal damping controlled system reaches $\bar{P}_{fd}$=220 kW (at global optimal damping of 1.75 Nm/(rad/s)) and $\bar{P}_{odc}$=224 kW respectively, resulting in a difference of 4 kW (only 2% of the power extraction from optimal damping control). The small difference is due to the low variability of the sea states at CN, where sea states mainly occur at peak wave period between 12 s and 14 s. As shown in Fig. 4, the optimal generator damping at these three peak wave periods are very close with a standard deviation of less than 0.5 Nm(rad/s). At the Sydney site, the global optimal damping for the fixed-damping system occurs at 2.75 Nm(rad/s) since the sea states mainly occur at around 9 s peak wave period. Although the sea state variability of the Sydney site is clearly higher than the sea state variability of the CN site, the difference in power loss percentage between the globally optimized fixed-damping system ($\bar{P}_{fd}$) and the optimal damping controlled system ($\bar{P}_{odc}$) is about the same for the two sites (2%). This is because at sea states with a peak wave period lower than 9 s, the optimal damping remains relatively constant for decreasing wave period. The results imply that in theory it is not necessary to implement adaptive passive damping control on a CETO system at the two sites investigated. A fixed generator damping can be globally optimized for a CETO system based on the past sea state occurrence probability of the site. However, if a CETO system operates

at a site with more variable peak wave periods ranging between 8 and 15 s, the effects of control will be more significant. In addition, it is worth noting that in reality, modelling error, sea state variability and longer-term climate change will lead to a lower power level for the fixed-damping system since its fixed 'global optimal' damping was purely computed from the WEC model and past sea state probability data, which is inherently an open loop method.

6. MPPT control of CETO

MPPT control is a non-model based feedback method and consequently adapts to sea state variability and model uncertainty. The efficiency of MPPT control though is governed by its tracking ability under irregular waves. This section describes a sensitivity study on the choice of step size and update rate for MPPT control on WEC, as well as on the number of averaging cycles sufficient for the optimization study conducted in Section 5. This section also investigates the performance of MPPT control on CETO.

6.1. Study on the sensitivity of control to irregular wave fluctuations

A sensitivity study was undertaken with the aim to understand the variability of WEC power output under an irregular incident wave, and consequently to select optimal settings (e.g. update rate and step size) for the MPPT controller to achieve the best absorption efficiency on the WEC. For each of the sea states investigated, a Pierson-Moskowitz spectra and 8 random phase vectors (each random phase vector consists of 1000 random phase components to match the spectra frequency components) were generated, resulting in 8 different time-series representation of the sea state that emulate the randomness or variability of irregular wave. During simulation, the generator damping coefficients were altered between 0.25 and 7.5 Nm/(rad/s) with increments of 0.25 Nm/(rad/s). Each case (e.g. sea state [2 m, 11 s], random phase vector 1, and generator damping 0.25) ran for 440 cycles of the peak wave period (e.g. $440 \times 11 = 4840$ s). Averaging of the instantaneous generated power was taken over 60, 180, 300, and 420 cycles of the peak wave period starting from the 20th cycle. The results associated with the sea state of 2 m significant wave height and 11 s peak wave period are shown in Fig. 12. The different color solid/dotted lines in each of the four subplots represent the averaged power generated against the generator damping coefficients associated with the different random phases. Each subplot shows the results averaged over a specific number of cycles of peak wave period (e.g. 60 cycles on the top left). Clearly, the variability in power output due to the randomness of irregular wave decreases with an increase in averaging cycles, which implies that for MPPT control to be effective, the update rate needs to be sufficiently slow to filter out variability in power output due to the randomness of irregular waves. The standard deviation (SD) of maximum variability in power output (at optimal damping) arising from different averaging cycles is shown in Table 3 for 4 typical sea states, as well as the SD of optimal damping coefficient. The SD of maximum variability in power output was also normalized to the maximum mean power generated (at optimal damping). The SD of power output due to wave fluctuations was found to diminish approximately exponentially with the increase of averaging cycles. On the other hand, the SD of optimal damping coefficient is not particularly sensitive to the cycle number for averaging. When averaging for 300 cycles, the maximum variability in power output is only about 3% of the maximum mean generated power, which is sufficiently accurate for the optimization study. Therefore, averaging over 300 cycles of peak wave period was used for the optimization study discussed in Section 5.

For MPPT control to be effective in irregular waves, the variability in the system mean power output due to irregular wave fluctuations needs to be smaller than the change in the system mean power output due to controllable variable change (e.g. in the case of CETO system, the change in generator damping) as shown in Eq. (27). This was assessed for the sea state of [2 m,11 s] and 420 averaging cycles (e.g. right bottom subplot in Fig. 12), and is illustrated in Fig. 13 with only the curve associated with random phase 2 displayed. At the optimal generator damping (2.75 Nm/(rad/s)), the SD of the variability in power output due to wave fluctuations (abbreviated as WF; shown as vertical red scale in Fig. 13) reaches a maximum, while the change in power output arising from change in generator damping with a step size of 0.25 (abbreviated as DC; shown as vertical black scale in Fig. 13) reaches a minimum. This leads to a much higher WF than DC. Therefore Eq. (27) is not satisfied leading to ineffective performance of MPPT control at the optimal generator damping. When the generator damping is further away from the optimal point, the smaller the variability in power output due to wave fluctuations, while the larger the change in power output arising from change in damping, resulting in two boundaries near the optimal point. Within such boundaries, WF is larger than DC so that MPPT control is not effective, while once outside such boundaries, WF is smaller than DC so that MPPT control becomes effective. Therefore, the region within these boundaries is defined as the MPPT ineffective zone, while the region outside these boundaries is defined as the MPPT effective zone. Clearly, the larger the step size for MPPT control, the larger the change in power output arising from the change in damping, and consequently the narrower the MPPT ineffective zone. On the other hand, MPPT control can make one step into the MPPT effective zone when working at the boundaries. As soon as in the MPPT effective zone, the controller will immediately move the generator damping back into the MPPT ineffective zone. Such one step into the MPPT effective zone is defined as control fluctuation zone, indicating oscillating behaviour of the controller at the boundaries of the MPPT ineffective zone. A larger step size causes the generator damping to step further into the MPPT effective zone, and consequently results in a larger control fluctuation zone. An uncertainty zone is defined to quantify the possible generator damping range under MPPT control (e.g. uncertainty zone is defined by the superposition of MPPT ineffective zone and control fluctuation zone as shown in Fig. 13). The maximum possible power loss (PL) of MPPT control arising from wave fluctuations is defined as the difference between the mean power output at optimal damping and the mean power output at the boundaries of the uncertainty zone, assuming the worst scenario that generator damping is oscillating repetitively at the boundaries of the uncertainty zone. The uncertainty zone associated with step size of 0.25, 0.5 and 0.75 Nm/(rad/s) is plotted respectively for sea state of [2 m, 11 s] is shown in Fig. 14, where the green region represents the uncertainty zone for a step size of 0.25, while the red region represents the uncertainty zone for a step size of 0.5 and 0.75. The range of the uncertainty zone and the maximum power loss arising from irregular wave variability are demonstrated in Table 3 for four typical sea states, with 420 cycles of averaging. For the sea state of [2 m, 8 s], a step size of 0.75 gives the best results with a maximum possible power loss of 4% of the maximum generated power. For the sea state of [2 m, 11 s], step sizes of 0.5 and 0.75 provide the same best results with a maximum possible power loss of 3%. For the sea state of [2 m, 14 s], a step size of 0.5 provides the best results with a maximum possible power loss of 2%. For the sea state of [4 m, 11 s], the results are similar with the results associated with sea state of [2 m, 11 s], which implies that the results are not sensitive to the change in significant wave height. Comparing the results for different peak wave periods, the optimal step size is clearly sensitive to the variation of peak wave periods. Therefore, the selection of step size needs to consider the sea state occurrence probability at the specific site. With regards to the selection of the update rate, an average over 420 cycles demonstrates effective results, however it is ideal to have a update rate as fast as possible to allow faster transient behaviour of the controller when sea state changes.

In the hydraulic PTO unit, the accumulators function like low-pass filters that are used to reduce the effects of incident wave variability on the extracted power. Assuming the volumes of the accumulators are

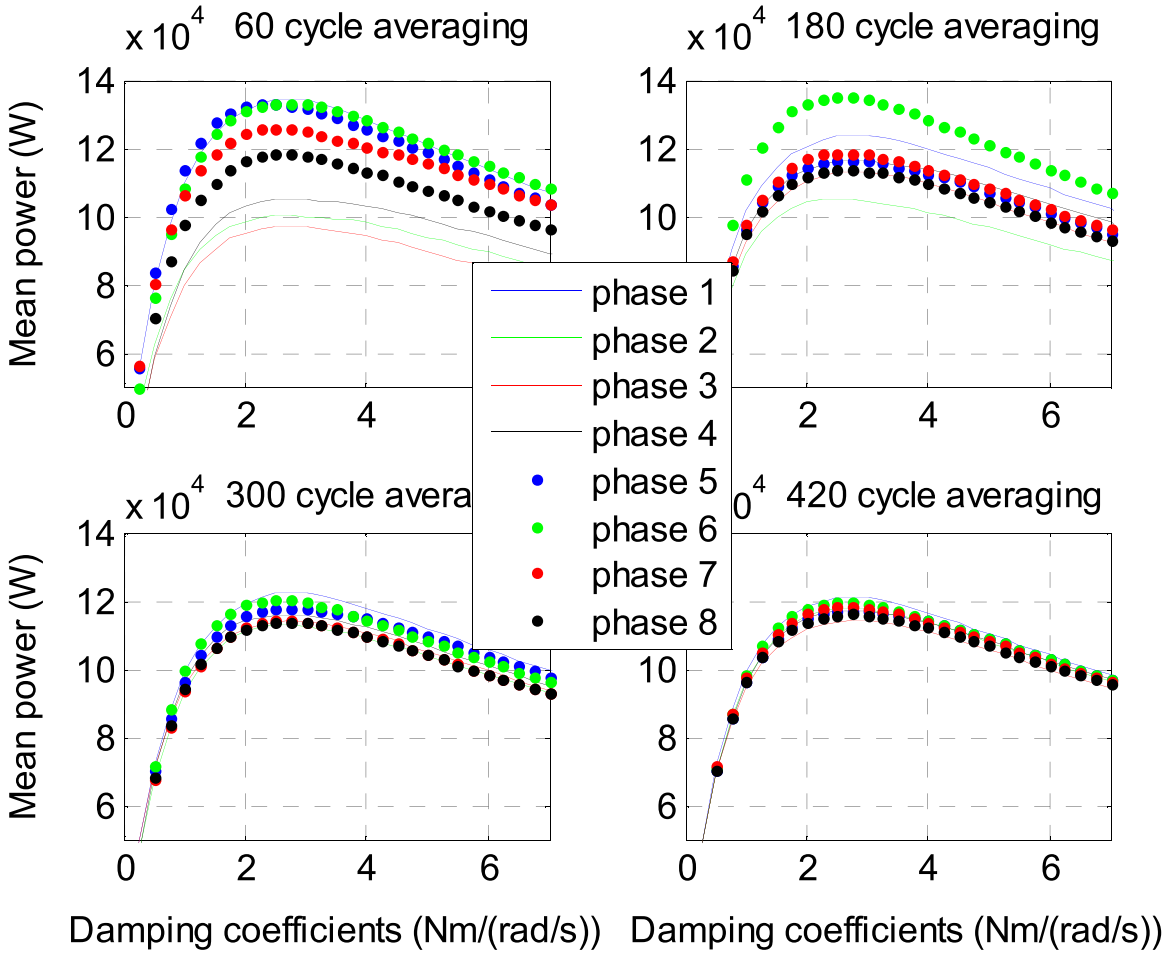

Fig. 12. The effects of variability in irregular waves (represented using eight different random phases) on WEC mean power output under various averaging duration. Sea state with 2 m significant wave height and 11 s peak wave period is used as an example here.

infinitely large, a constant pressure difference drives the hydraulic motor/generator at a constant speed, resulting in a constant power output. Therefore, it is intuitive that increasing the accumulator size can reduce variability in power due to wave fluctuations, resulting in improved performance of MPPT control (e.g. with faster update rate and narrower uncertainty zone). To assess this, the sensitivity study was repeated on the CETO model with four sets of high-pressure and low-pressure accumulator sizes subjected to the sea state of [2 m, 11 s]. The SD of normalized variability in system power output (at the optimal damping) for various accumulator sizes and averaging cycles is shown in Fig. 15. Results demonstrated that increasing the accumulator size does reduce the variability in system power output but not significantly. The full results associated with accumulator sizes of 20 m^3 are shown in Table 3. Compared with the case of 5 m^3

Table 3
Sensitivity study for various sea states.

Sea state (Hs; Tp)	SD of maximum variability in power output (kW) due to wave fluctuations and SD of optimal damping coefficient (Nm/(rad/s)) under various cycles of averaging								Range of uncertainty zone (Nm/(rad/s)) and maximum possible power loss (kW) under various step sizes for 420 cycles of averaging					
	60 cycle		180 cycle		300 cycle		420 cycle		0.25 step		0.5 step		0.75 step	
	PF	DV	PF	DV	PF	DV	PF	DV	UZ	PL	UZ	PL	UZ	PL
2 m; 8 s	16 (16%)	0.23	6.1 (6%)	0.13	2.7 (3%)	0.13	1.6 (2%)	0.13	2.25–7.5	> 9.7 (10%)	2.5–7	7.8 (8%)	2.75–5.75	3.5 (4%)
2 m; 11 s	15.6 (13%)	0.19	8.8 (8%)	0.13	3.4 (3%)	0.09	2.2 (2%)	0.09	1.75–4.75	10 (9%)	2–3.75	3 (3%)	2–3.75	3 (3%)
2 m; 14 s	12 (12%)	0.23	6.6 (7%)	0.13	3 (3%)	0	1.6 (2%)	0	1–2.5	3.8 (4%)	1–2.25	2.4 (2%)	0.75–2.25	6 (6%)
4 m; 11 s	78 (15%)	0.23	34 (7%)	0.09	14 (3%)	0.09	9.5 (2%)	0	1.5–3.5	28.7 (6%)	1.5–3	13.4 (3%)	1.5–3	13.4 (3%)
2 m; 11 s (20 m^3 accumulator)	11 (11%)	0.23	6.4 (6%)	0.13	2.6 (3%)	0.13	1.4 (1%)	0.09	2.25–6	7 (7%)	2.5–4.75	2.5 (2%)	2.5–4.5	2.4 (2%)
2 m; 11 s (capture width)	0.36 (6%)	0.19	0.26 (5%)	0.13	0.08 (1%)	0.09	0.07 (1%)	0.09	2–3.75	3 (3%)	2–3.5	2 (2%)	2–3.5	2 (2%)

*PF represents power fluctuation, DV represents damping variation, UZ represents uncertainty zone, and PL represents power loss, % presents the ratio of the value to the mean maximum generated power (at optimal generator damping) for the corresponding sea state.

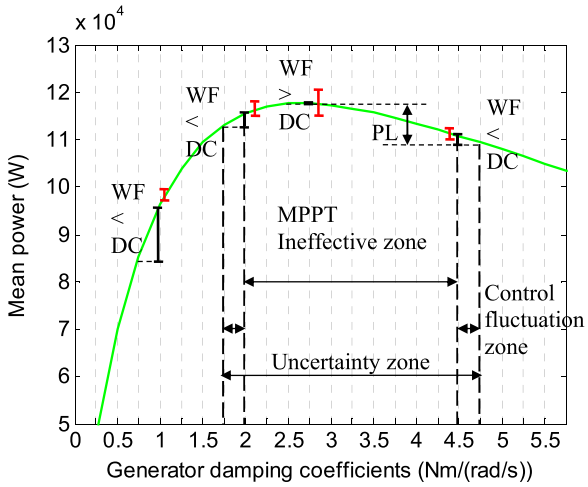

Fig. 13. Schematics comparing the variability in power due to irregular wave fluctuations (WF; shown as vertical red scales), with the power change due to generator damping change (DC; shown as vertical black scales) under MPPT control. A sea state with 2 m significant wave height and 11 s peak wave period is used as an example here, with 420 averaging cycles and a step size of 0.25 Nm/(rad/s) for MPPT control. PL presents the maximum possible power loss under MPPT control due to irregular wave fluctuations. (For interpretation of the references to color in this figure legend, the reader is referred to the web version of this article.)

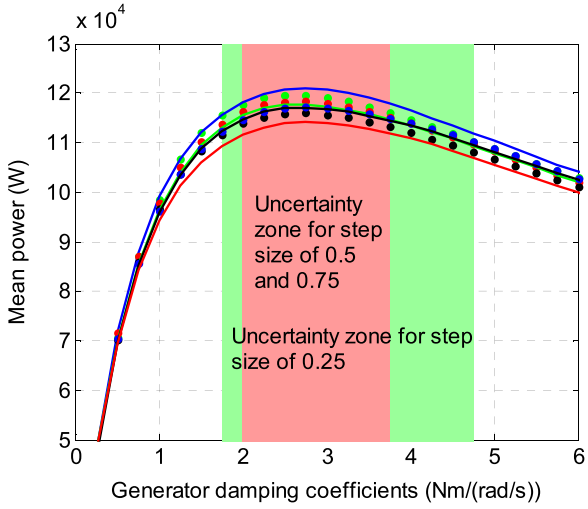

Fig. 14. MPPT control uncertainty zone for various step sizes: green region for step size of 0.25; red region for step size of 0.5 and 0.75. Sea state with 2 m significant wave height and 11 s peak wave period [2 m, 11 s] is used as an example here with 420 cycles of averaging. (For interpretation of the references to color in this figure legend, the reader is referred to the web version of this article.)

accumulators, the use of 20 m^3 accumulators improve the MPPT control efficiency by about 1%, which might not be significant enough compared to the additional cost employing larger accumulators to warrant their use. In addition, larger accumulators cause a larger time constant of the hydraulic PTO system, which has the potential to degrade the tracking performance of control.

As mentioned in Section 3, the mean capture width is a better measure of efficiency than mean power output for MPPT control, which is less sensitive to sea state variability. However, it is questionable if mean capture width is less sensitive to wave fluctuations/variability in a single sea state compared to mean power output. To assess this, energy transport (mean power) of incident wave averaged for a different number of cycles (e.g. 60, 180, 300 and 420) was calculated from the time series of incident wave elevation via the Fast Fourier Transform (Matlab *pwelch* function; 10 Hz sample frequency; 4096 point FFT; rectangular window; zero overlap) for each sea state. Divided by the energy transport of incident wave, the WEC mean

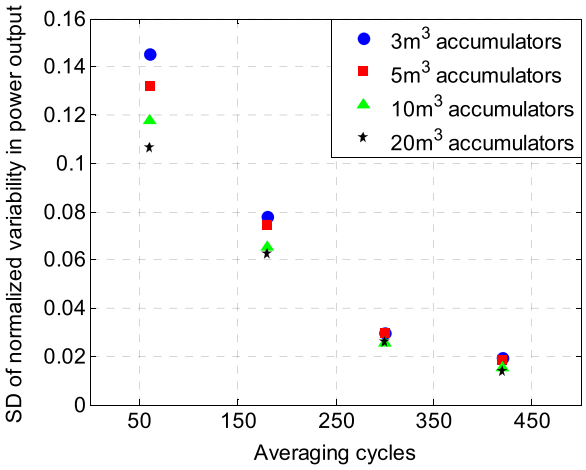

Fig. 15. SD of normalized variability in system power output for various accumulator sizes and averaging cycles. Sea state with 2 m significant wave height and 11 s peak wave period is used as an example here.

power output is normalized to give the mean capture width averaged at a different number of cycles. The same sensitivity study on WEC mean power output was repeated for mean capture width, assuming that the mean capture width is the target to optimise under MPPT control, with only the results associated with a sea state of [2 m, 11 s] shown in Table 3. Compared to the results for mean power output, the use of mean capture width does improve the performance, particularly for an average of 300 cycles, which implies that mean capture width is less sensitive to wave variability than mean power output in a single sea state, and consequently can be used to improve MPPT control with a faster update rate.

6.2. *MPPT control simulation*

Based on the results of the sensitivity study covered in Section 6.1, a step size of 0.5 Nm/(rad/s) and a update duration of 4620 s (1.28 h) were selected for the MPPT controller. In the hydraulic PTO Simscape model, the 'rotational damper' function block was replaced by an 'ideal torque source' function block that is driven by the coded MPPT controller with mean capture width as the optimization target. The generator damping starts low at 0.25 Nm/(rad/s). The propagation of generator damping under MPPT control and the resulting extracted mean power (e.g. averaged over each update duration) are shown in Fig. 16(a) and (b) respectively, for a single sea state of [2 m, 11 s]. Clearly, when the generator damping is not in the uncertainty zone, MPPT effectively drives the generator damping towards the optimal point. When the generator damping is in the uncertainty zone, the MPPT control exhibits slightly random behaviour, however the generator damping coefficient does not stay far from the optimal. A power uncertainty zone is defined in Fig. 16(b) to show the possible range of mean extracted power due to wave variability and MPPT control, assuming that the generator damping is controlled within the uncertainty zone. The red dashed line represents the acausal optimal mean power averaged over wave variability. Under MPPT control, the mean extracted power fluctuates near the acausal optimal mean power (116 kW) with a SD of 2.6 kW and a mean power of 115.8 kW.

The changes in generator damping under MPPT control is shown Fig. 17(a), for a sea state of [1 m, 14 s] linearly transitioning to a sea state of [2 m, 11 s] over one-hour period. When the sea state changes, MPPT control effectively drives the generator damping from the uncertainty zone of the previous sea state into the uncertainty zone of the new sea state. The resulting mean relative capture width of the system over time is shown in Fig. 17(b), which oscillates around the acausal optimal averaged value for each sea state.

In order to assess the global efficiency of the MPPT controlled

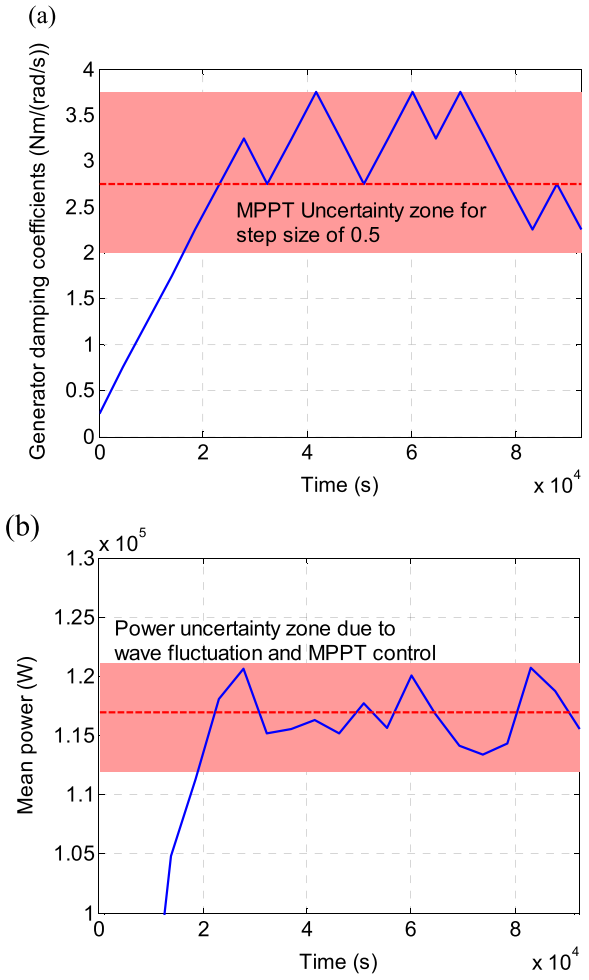

Fig. 16. Results under MPPT control for sea state [2 m, 11 s], with a update duration of 4620 s and a step size of 0.5 Nm/(rad/s). The uncertainty zones were obtained from Fig. 14. (a) Generator damping coefficients versus simulation time. The red region represents the MPPT uncertainty zone and the red dashed line represents the optimal damping. (b) Generated mean power versus simulation time. The red region represents the power uncertainty zone and the red dashed line represents the acausal optimal averaged mean power. (For interpretation of the references to color in this figure legend, the reader is referred to the web version of this article.)

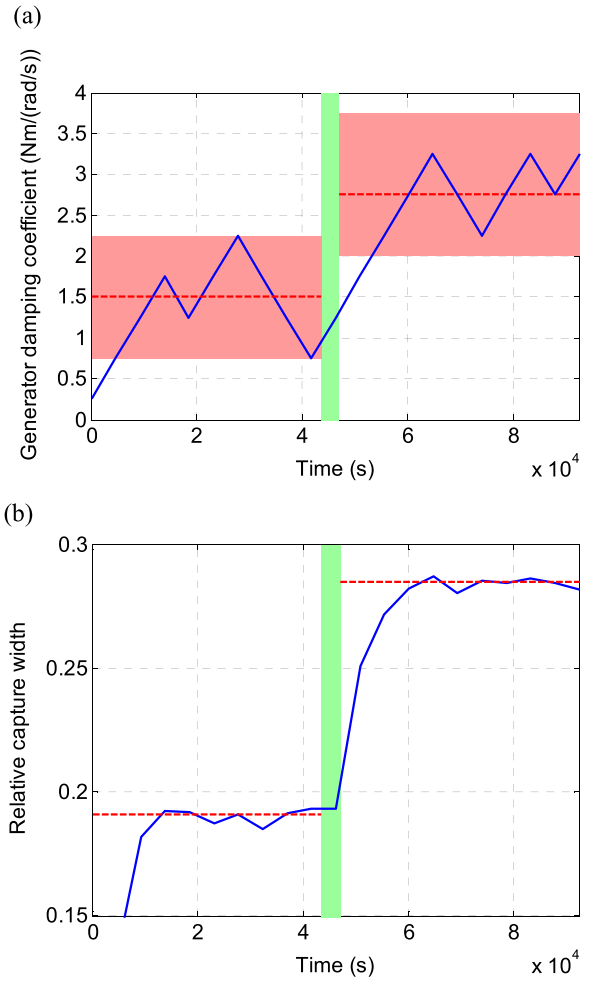

Fig. 17. Results under MPPT control for a sea state of [1 m, 14 s] transiting to a sea state of [2 m, 11 s], with a update duration of 4620 s and a step size of 0.5 Nm/(rad/s). The green region represents the one-hour transition period. (a) Generator damping coefficients versus simulation time. The red regions represent the MPPT uncertainty zones and the red dashed lines represent the optimal damping for each of the two sea states. (b) Mean relative capture width versus simulation time. The red dashed lines represent the acausal optimal averaged relative capture widths for the two sea states. (For interpretation of the references to color in this figure legend, the reader is referred to the web version of this article.)

CETO system, sea state time series during June 1997 at Sydney site was extracted for control simulation as shown in Fig. 18. The sea state time series was quantized to integers that were then transformed to segments of wave elevation time series for computing the excitation force. Standard linear interpolation over a 10 s period was implemented between each two segments to minimize unexpected nonlinear behaviour arising from sudden step changes in the excitation force when the sea state changes. The quantization of the sea state time series allows a fair comparison of the power absorption capacity of the MPPT controlled system with the analytically optimized fixed-damping system and acausal optimal damping controlled system. Results are populated in Table 4, with 98.8 kW averaged power ($\bar{P}_{fd}$) extracted from the globally optimized fixed-damping system, 92.7 kW ($\bar{P}_{sfd}$) for the suboptimal fixed-damping system, 99.4k W ($\bar{P}_{mppt}$) for the MPPT controlled system, and 101.4 kW ($\bar{P}_{odc}$) for the acausal optimal damping controlled system. The globally optimized fixed-damping system was operating at a fixed generator damping of 2.75 Nm/(rad/s), which was the global optimal point for the sea state time series. The suboptimal fixed-damping system was operating at a suboptimal generator damping of 1.5 Nm(rad/s) that was assumed to be caused by both modelling error and sea state forecast error in practice. Modelling error is mainly due to the assumption of linear wave theory (Rafiee and Fievez; Iversen, 1982). Sea state forecast error is subject to measurement accuracy of the device, sea state variability and longer-term climate change (Hemer and Griffin., 2010; Mackay et al., 2010). Clearly, the MPPT damping controlled system is 0.6% more effective than the globally optimized fixed-damping system, 6.7% more effective than suboptimal fixed-damping system, and 1.9% less effective than the acausal optimal damping controlled system. There are three main reasons that caused the global efficiency loss of the MPPT controlled system. Firstly, at 'steady-state' of a single sea state, the irregular wave variability made the generator damping fluctuate within the uncertainty zone as described in the sensitivity study. Secondly, it took time for the generator damping to shift between two optimal points during sea state change. Finally, the optimization target, capture width, was continuously disturbed by sea state change. Although capture width is much less sensitive than WEC power output to sea state change, as long as sea state varies fast enough, the changes in capture width will be dominated by the effects of sea state varying rather than by the effects of generator damping varying. During these circumstance, MPPT controlled system will be less effective.

7. Conclusion

A sea-state based maximum power point tracking (MPPT) control

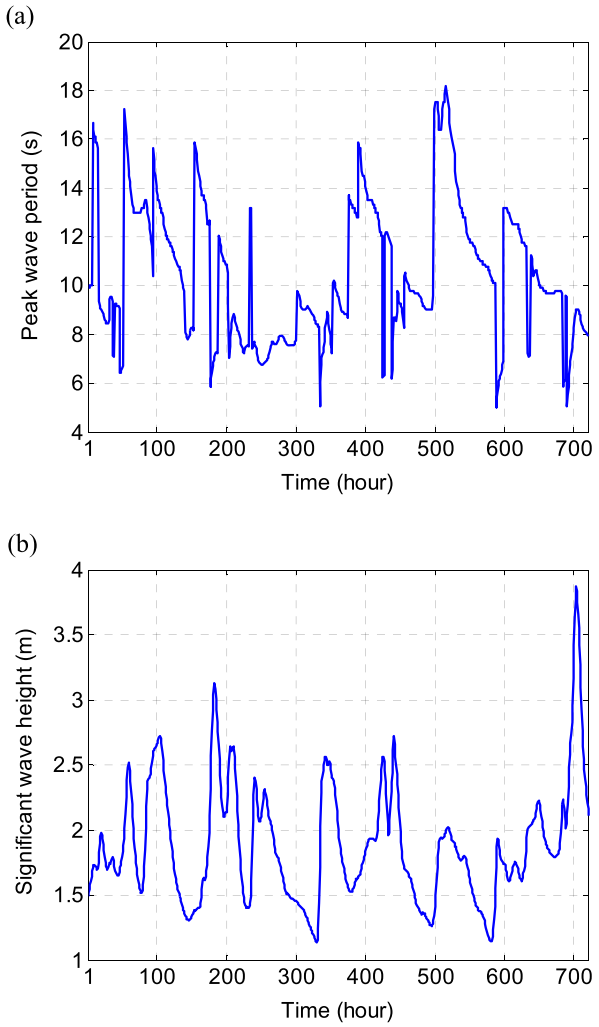

Fig. 18. Sea state time series during June 1997 at Sydney site. (a) Peak wave period versus time in hours. (b) Significant wave height versus time in hours.

Table 4
Comparison of averaged power extraction between fixed-damping system, MPPT controlled system and acausal optimal damping controlled system.

Methods	Fixed-damping system		MPPT controlled system, $\bar{P}_{mppt}$	Optimal damping controlled system, $\bar{P}_{ac}$
	Global optimal, $\bar{P}_{fd}$	Suboptimal, $\bar{P}_{fd}$		
Averaged power (kW)	98.8 kW	92.7 kW	99.4 kW	101.4 kW

algorithm was proposed for use on a fully submerged wave energy converter with a tether coupled hydraulic PTO. A sensitivity study was formulated to determine the step size and update rate of the MPPT controller, to ensure efficiency. The Carnegie CETO system was used as a test case to assess the proposed methodology, with generator damping as the control parameter. Results demonstrated that the optimal generator damping is sensitive to the change in the peak wave period but is not particularly sensitive to the change in the significant wave height. On the other hand, the optimal fluid volume of the hydraulic system is insensitive to the change in sea state, and therefore it is unnecessary to control the fluid volume. Results also demonstrated that the efficiency of CETO system with a globally optimized fixed PTO damping is close to the efficiency of acausal optimal damping control if the sea state probability is known in advance. However, when the modelling/forecast error is considered and sea state becomes more variable, the effects of damping control will become more significant.

A sensitivity study was conducted to determine the variance in PTO power output as a function of incident wave variability, as well as a function of PTO generator damping coefficients. A limited set of eight random phase vectors were used for the study mainly due to slow computational speed of the SimHydraulic model compared to pure analytical modelling. Issues with solver stiffness can arise for large sea states and inappropriate choice of generator damping. This happens because the fixed parameters of the hydraulic PTO system were only ever designed for the most frequent sea state, which is considerably smaller than the largest sea state investigated. A more comprehensive statistical study on the control sensitivity on an oscillating water column is discussed in detail in Hardy et al., 2016. The MPPT control simulation was conducted using the step size and update rate selected based on the sensitivity study, with mean capture width as the optimization target. Results matched with the expectation from sensitivity study. At 'steady-state' the MPPT control works effectively by keeping the generator damping around the optimal point but strictly within an uncertainty zone. The tracking ability and global efficiency of MPPT control was assessed based on a whole month time series of the sea state, which was compared to the efficiencies of the suboptimal/optimal fixed-damping system and the acausal optimal damping controlled system. Results showed that the MPPT controlled system extracts more power than the global optimized fixed-damping system. The efficiency of the MPPT controlled system is even greater when compared to the suboptimal fixed-damping system arising from modelling error and forecast error in practice. Passive damping control was considered in this paper given its simplicity and easy implementation in a generic hydraulic PTO unit, although its power extraction efficiency is lower than impedance matching and latching control techniques (Hals). The proposed sea-state based MPPT damping control method has the potential to increase the absorption efficiency of Carnegie's CETO system by 1–6%, which results in additional annual power extraction of up to 0.1 GW h per unit.

It is expected that sea-sate based MPPT control would be suitable to adapt latching duration for latching control. The investigation of MPPT based latching control on CETO system is under progress, taking system constraints (e.g. pressure capacity of the PTO unit and load capacity of the tether) and model uncertainty into consideration (Davidson et al., 2015). The disturbances arising from sea state variance will be modelled to study the sensitivity of control to sea state change. Future work also includes small/full scale experimental validation of the MPPT based methods.

Acknowledgement

The authors would like to acknowledge the financial support from Australian Research Council, Linkage Project LP130100117. The authors would also like to thank Dr Mark Hermer from CSIRO for providing the sea state time series along the Australian coast. In addition, the authors would like to acknowledge Mrs Nataliia Sergiienko from the School of Mechanical Engineering, the University of Adelaide, and Dr Ashkan Rafiee and Mr Jack Jorgensen from Carnegie Wave Energy for their assistance in modelling.

References

Amon, E.A., Brekken, T.K.A., Schlacher, A.A., 2012. Maximum power point tracking for ocean wave energy conversion. IEEE Trans. Ind. Appl. 48 (3), 1079–1086.
Babarit, A., Clement, A.H., 2006. Optimal latching control of a wave energy device in regular and irregular waves. Appl. Ocean Res. 28, 77–91.
Babarit, A., Hals, J., et al., 2012. Numerical benchmarking study of a selection of wave energy converters. Renew. Energy 41, 44–63.
Babarit, A., Guglielmi, M., Clement, A.H., 2009. Declutching control of a wave energy converter. Ocean Eng. 36, 1015–1024.
Bachynski, E.E., Young, Y.L., Yeung, R.W., 2012. Analysis and optimization of a tethered wave energy converter in irregular waves. Renew. Energy 48, 133–145.

Cargo, C.J., Plummer, A.R., Hillis, A.J., Schlotter, M., 2012. Determination of optimal parameters for a hydraulic power take-off unit of a wave energy converter in regular waves. J. Power Energy 226 (98), 98–111.

Carnegie Wave Energy. CWE Shareholder update. 15 October 2014.

Cummins, W.E., 1962. The impulse response function and ship motions. Schiffstechnik 9, 101–109.

Davidson, J., Giorgi, S., Ringwood, J.V., 2015. Linear parametric hydrodynamic models for ocean wave energy converters identified from numerical wave tank experiments. Ocean Eng. 103, 31–39.

Ding. B., Sergiienko, N., Meng, F., Cazzolato, B.S., Arjomandi, M., Hardy, P. Enhancing the relative capture width of submerged point absorbers. Ocean Engineering, under preparation.

Elmes, J., Gaydarzhiev, et al., 2007. Maximum energy harvesting control for oscillating energy harvesting systems. In: Proceeding of IEEE Power Electronics Specialists Conference, pp. 2792–2798.

Falcao, A.F., de, O., 2007. Modelling and control of oscillating-body wave energy converters with hydraulic power take-off and gas accumulator. Ocean Eng. 34, 2021–2032.

Falnes, J., 2007. Ocean Waves and Oscillating Systems. Cambridge University Press.

Hals, J., Falnes, J., Moan, T., 2011. A comparison of selected strategies for adaptive control of wave energy converters. J. Offshore Mech. Arct. Eng. 133, 301101-1-12.

Hals, J. Modelling a phase control to wave-energy converters (Doctoral Thesis). Norwegian University of Science and Technology.

Hardy, P., Cazzolato, B.S., Ding, B., Prime, Z., 2016. A maximum capture width tracking controller for ocean wave energy converters in irregular waves. Ocean Engineering 121, 516–529.

Hemer, M.A., Griffin, D.A., 2010. The wave energy resource along Australia's southern margin. J. Renew. Sustain. Energy 2, 043108.

Henderson, R., 2006. Design, simulation, and testing of a novel hydraulic power take-off system for the Pelamis wave energy converter. Renew. Energy 31 (2), 271–283.

Iversen, L.C., 1982. Experimental study of the deviation from linear behaviour for a submerged spherical point absorber. Appl. Ocean Res. 4 (1), 33–40.

Jiang, S., Gou, Y., Teng, B., Ning, D., 2014. Analytical solution of a wave diffraction problem on a submerged cylinder. J. Eng. Mech. 140 (1), 225–232.

Koutroulis, E., Kalaitzakis, K., 2006. Design of maximum power tracking system for wind-energy-conversion applications. IEEE Trans. Ind. Electron. 53 (2), 486–494.

Mackay, E.B.L., Bahaj, A.S., Challenor, P.G., 2010. Uncertainty in wave energy resource assessment. Part 1: Historic data. Renew. Energy 35, 1972-1808.

Perez, T., Fossen, T.I., 2009. A Matlab toolbox for parametric identification of radiation-force models of ships and offshore structures. J. Model. Identif. Control 30 (1), 1–15.

Rafiee, A., Fievez, J. Numerical prediction of extreme loads on the CETO wave energy converter. In: Proceeding of 11th European Wave and Tidal Energy Conference, 09A1-2.

Ringwood, J.V., Bacelli, G., Fusco, F., 2014. Energy-maximizing control of wave-energy converters. IEEE Control Syst. Mag., 30–55, (October).

Sergiienko, N., Cazzolato, B.S., Ding, B., Arjomandi, M., 2016. An optimal arrangement of mooring lines for the three-tether submerged point-absorbing wave energy converter. Renew. Energy 93, 27–37.

Snyder, S.D., 2000. Active Noise Control primer. Springer Verlag, New York.

Srokosz, M.A., 1979. The submerged sphere as an absorber of wave power. J. Fluid Mech. 95, 717–741.

van Dam, F.C., Gebraad, P.M.O., van Wingerden J., 2012. A maximum power point tracking approach for wind farm control. In: Proceedings of the Science of Making Torque from Wind Conference.

Vicente, P.C., Falcao, A.F.O., Justino, P.A.P., 2013. Nonlinear dynamics of a tightly moored point-absorber wave energy converter. Ocean Eng. 59, 20–36.

Xiao, W., Dunford, W.G., Palmer, P.R., 2007. Application of centered differentiation and steepest descent to maximum power point tracking. IEEE Trans. Ind. Electron. 54 (5), 2539–2549.